Archives of Agriculture and Environmental Science 9(4): 691-698 (2024)
https://doi.org/10.26832/24566632.2024.090408

e-ISSN: 2456-6632

This content is available online at AESA

Archives of Agriculture and Environmental Science

Journal homepage: journals.aesacademy.org/index.php/aaes

ORIGINAL RESEARCH ARTICLE

Urban heat island relation with land use land cover change in Hetauda sub-metropolitan city of Nepal

Bikram Singh[1,2], Gayatri Paudel[2], Amrit Thapa[3], Hem Chandra Joshi[1] and Menuka Maharjan[2,4*]

[1]Far Western University, Faculty of Natural Resource Management, Kailali Multiple Campus, Kailali, Nepal
[2]Tribhuvan University, Institute of Forestry, Hetauda Campus, Makwanpur, Nepal
[3]Geophysical Institute, University of Alaska Fairbanks, Fairbanks, AK 99775, USA
[4]School of Forestry and Natural Resource Management, Institute of Forestry, Tribhuvan University, Kathmandu, Nepal
*Corresponding author's E-mail: menuka48maharjan@gmail.com

ARTICLE HISTORY

Received: 23 September 2024
Revised received: 17 November 2024
Accepted: 27 November 2024

Keywords

GIS
NDVI
NDBI
Remote sensing
Spatio-temporal

ABSTRACT

Urban areas are expanding globally at the expense of natural productive land which affects the quality of life of urban residents. Hetauda sub-metropolitan city of Nepal has been undergoing rapid urban growth for the last few decades causing local climatic effects such as land surface temperature (LST) variation. Thus, exploring spatio-temporal changes in land use, land cover (LULC), and urban heat island (UHI) analysis could be an effective means of exposing local environmental issues caused by anthropogenic activities. Development in thermal Remote Sensing and Geographic Information System (GIS) has enabled the monitoring of spatial LST, UHI, and its correlation to LULC. We used Landsat 8 OLI/TIRS satellite data and a supervised classification algorithm for land use land classification for the years 1995, 2008, and 2018 in Arc map software. The spatial pattern of LST was obtained through mathematical calculation of the thermal band of Landsat images. Correlation analysis was applied to explore the relationship between LST, LULC types, and LUCL indices. The LST was higher for urban/built-up and cultivated land use types. There was approximately 4°C mean LST variation for all three years of study. The regression analysis showed a positive correlation of urban/built-up with the Normal Difference Built-Up Index (NDBI) however a negative correlation with the Normal Difference Vegetation Index (NDVI) which implies that green structure weakens the UHI effects while urban/built-up areas strengthen the UHI. Overall, the study can be useful for urban planners in sustainable urban planning and management as well as to raise public awareness of climate change and the warming effect.

Citation of this article: Singh, B., Paudel, G., Thapa, A., Joshi, H. C., & Maharjan, M. (2024). Urban heat island relation with land use land cover change in Hetauda sub-metropolitan city of Nepal. *Archives of Agriculture and Environmental Science*, 9(4), 691-698, https://dx.doi.org/10.26832/24566632.2024.090408

INTRODUCTION

Urban Heat Island (UHI) is the result of a combination of factors, including a higher proportion of absorbed radiation from the sun than latent heat forms, a greater capture of infrared radiation within roadway canyons, a greater absorption and slower emission of thermal energy from constructed structures, and more release of latent heat from burning fuels for processing in factories, urban transportation, and residential heating systems (Stewart & Oke, 2012). UHI is a geographical area that is warmer than its surroundings due to the earth's surface features and was first used by Howard in 1833 (Laosuwan & Sangpradit, 2012; Nuruzzaman, 2015). The spatial variation of landscape cover causes variation in Land Surface Temperature (LST) with the surrounding area of the impervious zone thus resulting in the formation of UHI (Ranagalage *et al.*, 2017; Singh *et al.*, 2017). UHI appears based on LST as governed by surface heat fluxes and impervious objects. Spatial LST is the first step of UHI analysis (Singh *et al.*, 2017). According to Hokao *et al.*, 2012, LST corresponds to the outermost temperature at the land surface,

which is different from the surface air temperature. Since the pre-industrial era (1850-1900), the LST of air has been elevated globally by 1.53 °C (Shukla *et al.*, 2019). Due to the reduction of green space, diminishing water bodies, decreasing agriculture, and increasing impermeable surface, the temperature disparity between urban and rural environments has increased (Ranagalage *et al.*, 2018; Sharma *et al.*, 2015). Anthropogenic pressure resulting in rapid change in land cover in recent times and changing landscape patterns affects LST at the local level (Ghosh & Porchelvan, 2018).

Land use land cover change (LULC) dynamics play a crucial role in climate change at global and local levels (Tafesse & Suryabhagavan, 2019) LULC knowledge is crucial for understanding urban dynamics, including geology, topology, ecology, and sustainability, as well as land use patterns, urban density, urban diversification, and the phenomenon of UHI (Li *et al.*, 2018). LULC indices i.e. NDVI (Normal Difference Vegetation Index) for vegetation (West *et al.*, 2018), NDBI (Normal Difference Built-Up Index) for the built-up area (Bhatti & Tripathi, 2014; Zha *et al.*, 2003), and NDWI (Normal Difference Water Index) for water content area (Gao, 1995) are the best methods for extraction of LULC characteristics. Many scientific researches on urban heat effects have shown a strong connection between environmental variables and UHI (Clinton & Gong, 2013; Grigoraș & Urițescu, 2019). Remote sensing and geographical information systems (GIS) have emerged as essential tools in monitoring and analyzing urban LULC changes and their effects on LST. These technologies facilitate a comprehensive assessment of urban growth patterns and their environmental consequences (Tali *et al.*, 2013). For instance, the integration of remote sensing data allows for the evaluation of LST variations over time, enabling researchers to examine the links between land cover types and surface temperature (Jiang *et al.*, 2010; Sahana *et al.*, 2016). As remote sensing technology is quick, reliable, and cost-effective, scientific methods for land cover change and UHI analysis are very useful in developing countries like Nepal.

Nepal is a developing country and is considered as the fastest urbanization country in South Asia (Muzzini & Aparicio, 2013). Assessments of expanding urban history in Nepal since the late 1950s (Thapa & Murayama, 2009) revealed that city areas have grown swiftly. Hetauda sub-metropolitan city is one of the largest cities in Nepal constituting a population of 195,951 in 2021 (CBS, 2021). The city's development accelerated after it was named the district's capital in 1982. While the urbanization and LULC change processes in some cities of Nepal have already been studied, however, didn't include the Hetauda sub-metropolitan city (Rimal *et al.*, 2018). Since the city has grown plant species on both sides of the roads, it is additionally recognized as a "Green City" and is host to Nepal's greatest industrial area. However, LULC's contribution to the amplification of LST of the Hetauda sub-metropolitan city is still unknown due to the absence of research. Hence, this research aims to analyze the spatio-temporal changes of LULC and the associated UHI effect in Hetauda Sub-Metropolitan City by employing remote sensing and GIS technologies. By providing insights into the dynamics of urbanization and its climatic implications, this study aims to inform urban planning and management strategies that promote sustainable development in the region.

MATERIALS AND METHODS

Study area

The study area was the Hetauda sub-metropolitan city, Makawanpur district, Province No. 3, Nepal with an area of 261.65 km^2. It is located 345 meters above sea level at a latitude and longitude of 27°25' N and 85°02' E, respectively. Hetauda experiences tropical and subtropical weather, with warmer summers and colder winters. In the months of June through July and August, Hetauda has significant rainfall (Bhuyan *et al.*, 2013). The forest cover of Hetauda is 48.28 % (DFRS, 2015). About 153,875 people were living there as per the 2011 Nepal census (CBS, 2011). One of Nepal's largest industrial areas is the Hetauda Industrial District (HID), which is home to big, small to medium-sized and cottage industries.

Data used

Landsat satellite data from the Landsat 5 Thematic Mapper (TM) and Landsat 8 Operational Land Imager (OLI), obtained on April 7, 1995, April 10, 2008, and April 22, 2018, respectively, were used in this study. These Landsat data are accessible at no charge through the USGS portal and enhanced by NASA to produce Level-1 deliverables that have radiometric calibration and atmospheric correction methods (http://earthexplorer.usgs.gov/). Satellite photos were used from the summer months of April for 1995, 2008, and 2018 to ensure better comparability of surface temperature and the UHI effect. Due to their high geographical, spectral, and temporal precision, LANDSAT images are among the most frequently used satellite remote sensing data (Townshend, 2001). Shapefiles, which were provided by the Department of Survey, Hetauda, Makwanpur, were used to extract the area of interest in addition to the LANDSAT data.

Software used

ArcGIS was primarily used for the majority of spatial studies, including the identification of changes, urban expansion, LST measurement, and UHI evaluation. R programming was carried out for pixel value extraction which was used for correlation analysis. Google Earth was used to support the classification accuracy. Besides, MS Office packages, SPSS used for tabulation and visual representation of the results.

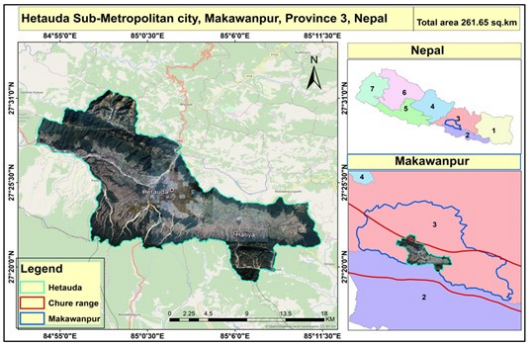

Figure 1. *Study area map.*

Data preparation

Digitally unprocessed photographs typically have inaccuracies brought on by changes in height, the curvature of the earth, and air refraction. Although they were employed in this investigation, Level-1 Landsat standard products are free of errors from the abovementioned sources (http://earthexplorer.usgs.gov/).WGS 1984 and UTM zone 45 N were used as the dataset's spatial reference systems. The necessary bands were combined with the entire image. Ultimately, the area of interest was extracted from Landsat photos by clipping them.

Methods

The many strategies used to achieve the aforementioned aim and objectives are condensed in this section. Concerning the application of a spatial-temporal land class change in our case, the UHI phenomenon approaches serve as excellent examples of the practical implications of GIS and remote sensing. Supervised maximum likelihood classification, change detection assessment, UHI analysis, and their interactions are the main methodologies used in our study.

Supervised maximum likelihood classification

The study area was divided into various LULC groups using supervised maximum likelihood classification. By using training samples for this method, it was possible to distinguish the spectral properties of the classes. This approach was greatly aided by knowledge in the relevant field. After gathering training samples, the Maximum Likelihood categorization algorithm was used to validate the categorization of the images. According to Tempfli *et al.* (2009), the approach assigns a cell to the class with the highest probability, where the probability value is the statistical distance based on the clusters' mean values and covariance matrix (Tempfli *et al.*, 2009). This categorization contains the five groups i.e. Forest, Cultivated land, Urban/built-up, Sand, and Water.

Table 1. LST retrieval steps.

S. No.	Step	Formula
1.	Conversion of digital number to radiance	$For\ Landsat8$ $L_\lambda = \frac{(LMAX\lambda - LMIN\lambda)}{(QCALMAX - QCALMIN)} \times (QCAL - QCALMIN) + LMIN\lambda$ $For\ Landsat\ 5$ $L_\lambda = MLQcal + AL - o_i$
2.	Conversion of radiance to At-Satellite temperature	$T = \frac{K_2}{ln\, ln(\frac{K_1}{L_\lambda} + 1)}$
3.	Conversion of Kelvin to Celsius	$BT = T - 273.15$
4.	Retrieving of land surface emissivity	$e = 0.004 \left(\frac{NDVI - NDVImin}{NDVImax - NDVImin}\right)^2 + 0.986$
5.	Land Surface Temperature (LST)	$LST = \frac{BT}{\left\{\left(1 + \frac{w \times BT}{(p = \frac{h \times c}{s})}\right) \times ln\, ln(e)\right\}}$

*L_λ=Spectral Radiance at the sensor's aperture in watts/(meter squared × ster × μm);LMINλ =the spectral radiance that is scaled to QCALMIN in watts/ (meter squared × ster × μm) LMAXλ =the spectral radiance that is scaled to QCALMAX in watts/(meter squared × ster × μm) QCALMIN =the minimum quantized calibrated pixel value (corresponding to LMINλ) in DN; QCALMAX =the maximum quantized calibrated pixel value (corresponding to LMAXλ) in DN; QCAL =the quantized calibrated pixel value in DN; ML=Band-specific multiplicative rescaling factor from the metadata (RADIANCE_MULT_BAND_x, where x is the band number), AL=Band-specific additive rescaling factor from the metadata (RADIANCE_ADD_BAND_x, where x is the band number), Qcal =Quantized and calibrated standard product pixel values (DN) and o_iis the correction for Band 10 (Barsi et al., 2014). T=Top of atmosphere brightness temperature (K), K_1=Band-specific thermal conversion constant from the metadata (K1_CONSTANT_BAND_x, where x is the thermal band number), K_2=Band-specific thermal conversion constant from the metadata (K2_CONSTANT_BAND_x, where x is the thermal band number, NDVI min=minimum value of NDVI, NDVI max=maximum value of NDVI, BT=at satellite temperature, w=wavelength of emitted radiance, h=plank's constant (6.626 × 10-34 JS), s=Boltzmann constant (1.38 × 10-23 J/K), c=velocity of light (2.998 × 10-8 m/s and p=14380.

Accuracy assessment

In general, classification-based LULC maps contain some mistakes as a result of a variety of circumstances, from the original data-collecting process to the application of the classification technique. Therefore, it is required to evaluate the accuracy of the categorization findings. The error matrix (confusion matrix) is the approach that is most frequently used to assess accuracy. An error matrix is a table with numbers in it that, when arranged in rows and columns, show the number of samples that were, concerning the truth, attributed to each classification. The LULC maps obtained via classification are represented in the matrix's rows, while the fieldwork-gathered reference data are shown in the matrix's columns. The kappa coefficient, error of omission and commission, and other statistical measures can be computed with the help of this matrix (Congalton, 2001). To obtain classification accuracy for this investigation, a confusion matrix was created.

LST retrieval

According to Rajeshwari & Mani (2014), LST is the temperature experienced when touching the ground with one's hands or the skin temperature of the ground. LST has been a major topic for creating approaches to be assessed from space since it is one of the most significant features of the land surface. LST is a significant consideration in many scientific fields, including studies of the global climate, farming and hydrological phenomena, and land use and cover in cities. Since LST is a crucial element influencing the majority of our planet's physical, chemical, and biological systems, it is necessary to calculate LST from remote sensed images (Rajeshwari & Mani, 2014). A series of steps are involved in LST retrieval (Table 1) (Haylemariyam, 2018):

UHI

According to Kaplan *et al.* (2018) and Ma *et al.* (2010), the UHI was detected using the following method in this study:

LST>m+0.5d Referred to UHI area
LST>m+0.5d Denoted non-UHI or rural area

Where 'm' and 'd' stand for the research area's mean and standard deviation of temperatures, respectively.

LULC indices

To evaluate the association between vegetation and built-up

area with LST, the NDVI and NDBI indices were calculated. Based on the following expressions, these indices were derived from the satellite images:

$$NDVI = \frac{NIR-R}{NIR+R}$$ (Rouse *et al.*, 1974)

$$NDBI = \frac{MIR-NIR}{MIR+NIR}$$ (Zha *et al.*, 2003)

Red, Near Infrared, and Mid-Infrared bands, respectively, are denoted by R, NIR, and MIR.

Relationship between vegetation indices and built-up index with LST

The relationship is based on pixel-based values of indices with the pixel value of LST. For this sixteen thousand nineteen pixel values were selected systematically having a confidence level of 99% for each land class indices for each study area to cover the whole area spatially. Thus correlation value was here calculated for vegetation indices and built-up area indices with LST.

RESULTS AND DISCUSSION

Accuracy assessment

The user, producer, and overall accuracy were obtained for 1995, 2008, and 2018. On this note, the overall classification accuracy in 1995, 2008, and 2018 was at 94.26%, 92.25%, and 92.91%, respectively. Besides kappa coefficients were 0.93, 0.95, and 0.91 for 1995, 2008, and 2018, respectively.

LULC

The findings of this study showed that Landsat satellite imagery is an excellent remote sensing technique for detecting LULC change and estimating the impact of UHI in both time and space (Singh *et al.*, 2017). The study elucidated that the way land was being used can directly affect how much heat is released. Also, forest cover gained slightly within 23 year period (1995-2008) i.e. 2.19 km^2 increased in the first interval (1995-2008) and 0.48 km^2 increased in the second interval (2008-2018). This study demonstrated that there had been a significant shift in the land use in the Hetauda sub-metropolitan city over the past 23 years (from 1995 to 2018), with the widespread growth of industrial land at the expense of agricultural land and to a lesser extent vegetation land due to heavy urbanization. The study area comprises 38 community forests (among them 36 established in the 1990s), which play a major role in forest restoration and could contribute to raising the forest cover in the study site (Division Forest Office, Hetauda). The forest cover increment in the study area is consistent with the national-level forest cover increment in the country (DFRS, 2015). Contrary, cultivated land decreased continuously within the study period by 7.38 km^{2}in 1995-2008 and by 4.18 km^2 in 2008-2018 periods (Figure 1) due to the conversion of those lands into built-up areas for a growing population. The urban/built-up area rose by 8.64 km^2 between 1995 and 2008, and 6.26 km^2 between 2008 and 2018 (Figure 1). This might be due to the consequence of population growth (www.citypopulation.de.) in the study area. Visual presentation of LULC map of Hetauda city for three years 1995 (A), 2008(B) and 2018(C) can be visualized (Figure 2). Statistically urban/built-up area increased by 8.64 km^2 in the first study period (1995-2008) and by 6.26 km^2 in the second study interval (2008-2018).

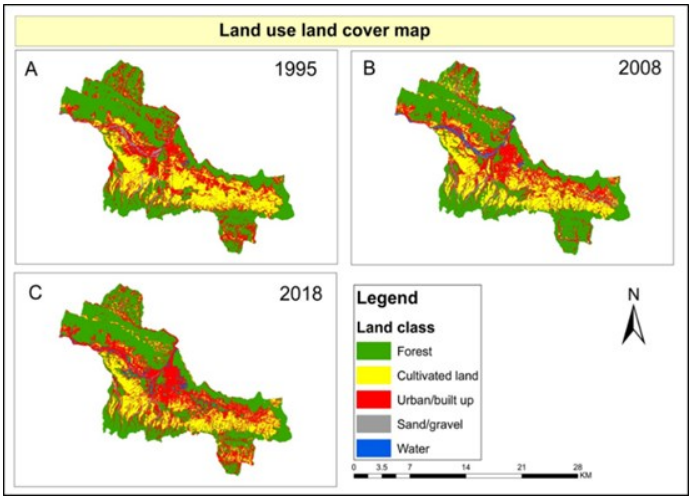

Figure 2. *Land use land cover map.*

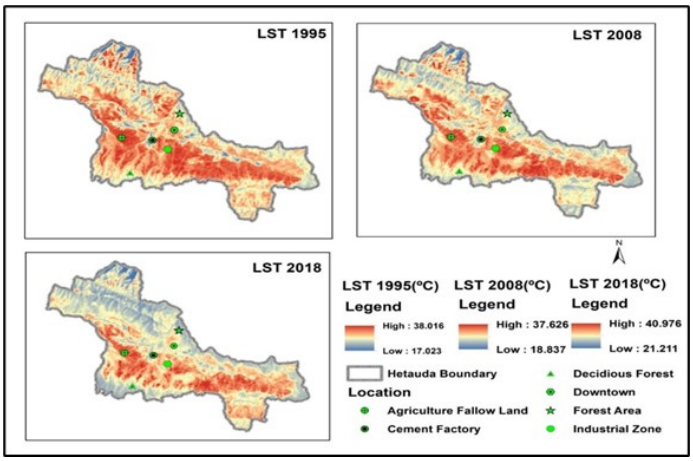

Figure 3. *Spatial LST map for 1995, 2008, and 2018.*

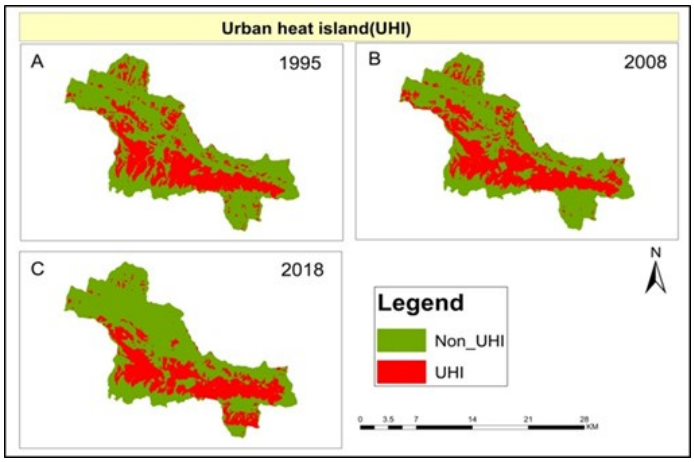

Figure 4. *UHI and non-UHI for 1995, 2008 and 2018m.*

LST Distribution map and UHI formation

The spatio-temporal map of LST is mapped for each year i.e. 1995, 2008, and 2018 (Figure 3), and mean LST was determined. The lower limit, upper limit, and mean LST for three periods (1995-2008, 2008-2018, and 1995-2018) were estimated. Hence mean LST difference for the years 1995 and 2008 decreased by 0.123°C and increased by 1.152 °C for the latter period of 2008-2018 and increased for the 1995-2018 year period. The mean LST was increased by 1.029°C between 1990-2018. Furthermore, a lower range of LST increased by 4.188°C whereas the upper range by approximately half of the lower ranges i.e., 2.961°C (Table 3). The LST distribution is more at the industrial zone, main downtown, and agriculture fallow land but forest land cover possesses less LST as compared to other classes (Figure 3). The LST distribution was more in the industrial zone, main downtown, and agriculture fallow land (Figure 3) but forest land cover possesses less LST as compared to other classes (Sarif *et al.*, 2020). The rate of increment of LST per decade (Sarif *et al.*, 2020) is quite similar to our findings of LST of 1995 and 2018 (Table 3). The UHI becomes more pronounced and the temperature gaps between urban and rural areas get larger (Heinl *et al.*, 2015). The UHI of Hetauda sub-metropolitan city was found to be much warmer than the nearby rural areas; as urbanization increased (Table 3). The UHI and no-UHI of Hetauda City were identified based on LST distribution (Figure 4) for each study year 1995, 2008, and 2018 (Figure 6). Thus, the UHI area in 1995, 2008, and 2018 was 83.78 km^2, 88.97 km^{2,} and 80.52 km^2 respectively. The mean LST for UHI for each year 1995, 2008, and 2018 varied i.e. 33.18°C to 32.78°C between 1995-2008 and 32.78°C to 34.48°C between 2008-2018 (Table 2). Similarly, mean LST for Non-UHI was 28.55 °C, 28.43 °C, and 29.54 °C for each year 1995, 2008, and 2018 respectively (Table 2). Interestingly, the mean LST of UHI and Non-UHI found a significant difference i.e. about 4°C for each year (Table 2) which is called the UHI effect. From the visual analysis of the map, UHI was also mainly concentrated in an industrial area, the main downtown, and agriculture fallow land (Figure 4). The output of this study is in line with research conducted by Li *et al.* (2020) in Hefei, China, that the expansion of UHI is directly proportional to LST and rapid urban growth i.e. unmanaged LULC dynamics. The UHI effect was realized by 4°C LST different for urban and peri-urban areas (Table 2). Hence the proper proportion of land use system should exist in metropolitan cities for sustaining cities and maintaining UHI adverse effects.

The UHI area in 2018 decreased to 80.52 km^2 (Table 6) from 88.97 km^2 in 2008 with the gradual increment of forest cover in 23 years (Figure 2) due to green vegetation, lowers LST which is beneficial to minimize UHI effects in urban areas (Rousta *et al.*, 2018). These findings imply that UHI has become more severe at all times as a result of the rise in industrial land at the expense of vegetation land and agricultural land which is expected to have detrimental effects on the local ecosystem. The detrimental consequences of stressors like climate change can be mitigated by using sustainable land management techniques (Ghosh & Porchelvan, 2018). Consequently, new greening measures must be devised, and lowering runoff including increasing the accessibility of freshwater by constructing lakes and ponds and harvesting rainwater. Such constructions can increase the adaptability of nearby environments (Santos & Gerry, 2017). Additional pressure on public or private authorities at the local and national levels to abate the UHI phenomenon from the implementation of measures to lessen its effects as well as enhancing the long-term sustainable strategy for emerging urban places may result from widespread knowledge of the severe effects of the UHI phenomenon (Rousta *et al.*, 2018).

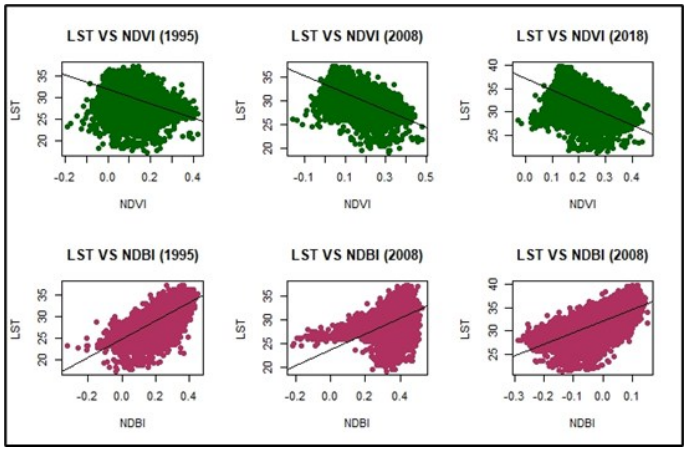

Figure 5. *Scatter plot of LST with NDVI and NDBI.*

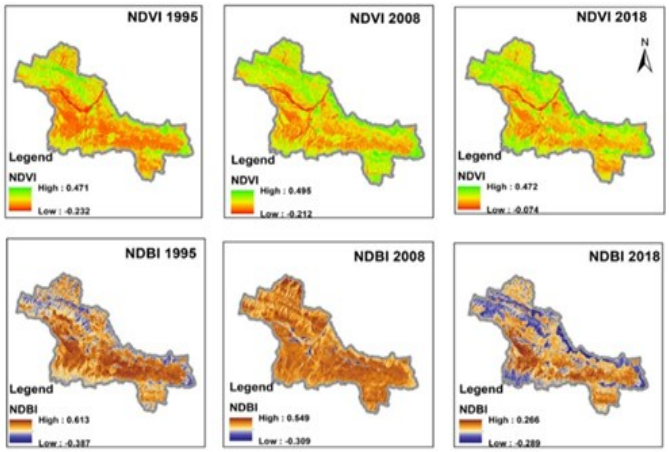

Figure 6. *NDVI and NDBI spatial pattern map for 1995, 2008 and 2018.*

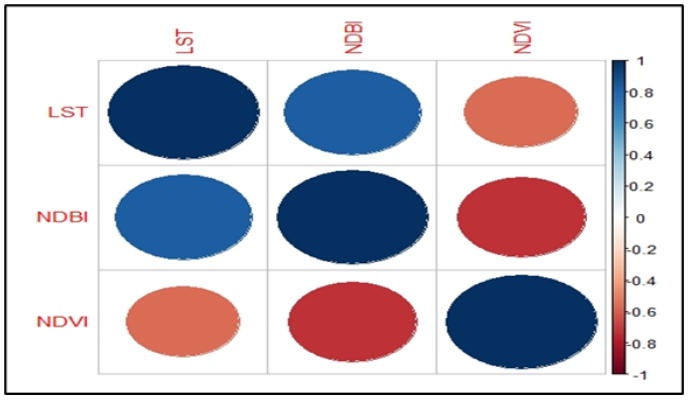

Figure 7. *Correlation of LST with NDVI and NDBI.*

LST and its relationship with LULC

The linkage between LULC and surface temperature indicators has been the subject of prior studies (Agam *et al.*, 2007; Agrawal *et al.*, 2008; Fernández *et al.*, 1997; W. Li *et al.*, 2015; Wu, 2004). For various land class features, the connection between LST and LULC indices can vary (Tariq *et al.*, 2020). Forest had mean LST in 1995 was 28.425°C, decreased to 28.241 °C in 2008, and eventually increased to 29.16 °C in 2018 (Table 3). The mean LST of cultivated land in 1995 was 32.513 °C, decreased to 32.416 °C in 2008, and finally increased to 34.500 °C in 2018. This showcases that agricultural land and forests experienced an increment in mean LST variations from 1995 to 2018. Variations in forest cover/density are related to variations in LST (Xu *et al.*, 2011). The mean LST of urban/built-up area increased i.e. from 30.129 °C in 1995, 30.765 °C in 2008, and 31.700 °C in 2018. Similar mean LST variations between urban/built-up areas and forests were discovered in the years 1995, 2008, and 2019. It was probably brought on by the influx of numerous residential communities, business growth, and adjacent districts throughout the year in the study site. The mean LST of the forest class increased by 0.735°C over the 23 years (1995-2018) period, cultivated land increased by 1.987°C, and urban/built-up area increased by 1.571° C which accorded with the findings of Xiong *et al.* (2012), who found that extreme temperatures variations are strongly correlated with developed land, densely populated areas, and heavily industrialized areas. It has been established that each land class has a different shift in mean LST. The mean LST change for forests throughout the 23-year (Table 3) has been lower than for other classes (Tariq *et al.*, 2020). It has been clear that the change in mean LST is varied for each land class. The mean LST change in the 23 years (1995-2018) for the forest is lower than for other classes. Furthermore, the cross-comparison of mean LST for each land class was determined. Thus there was a mean LST variation of 4.008°C, 4.174°C, and 5.34°C cultivated land and forest in 1995, 2008, and 2018 respectively. Similarly mean LST variation between urban/built-up areas and forest was found at 1.704°C, 2.524°C, and 2.54°C in 1995, 2008, and 2019 years, respectively.

NDVI and NDBI pattern and its relation with LST

The correlation between LST and NDVI was negative while NDBI was found positive for three study years (Figure 5). The correlation coefficient between LST and NDVI was found -0.479, -0.655, and -0.639 in 1995, 2008, and 2018, respectively (Figure 7). The correlation coefficient of LST between NDBI was found 0.779, 0.436, and 0.775 in 1995, 2008, and 2018, respectively (Figure 7). The study carried out in Tehran city of Iran found that negative correlation between LST with NDVI and a positive correlation with NDBI (Haylemariyam, 2018; Jamei *et al.*, 2019; Rousta *et al.*, 2018) which is similar to our result (Figure 7). The negative relationship between LST and NDVI indicates the green vegetation cover lowers the warming effect while the positive relation between LST and NDBI indicates the built-up area raises the local warming effect. Compared to forest land and water bodies, other land use had a high surface temperature (Table 3) because other land use such as built-up area, and bare and cultivated land promotes the surface temperature and makes the surroundings warm (Rousta *et al.*, 2018). Increased development activities in one location have led to the loss of potential natural places, which makes climate change actions even more dangerous (Gillespie *et al.*, 2018). The mean NDVI value increased during the study period i.e. 0.116 in 1995, 0.194 in 2008, and 0.242 in 2018 (Table 4). The mean NDBI increased in the period (1995-2008) from 0.247 to 0.377 while decreased in the later interval (2008-2018) i.e. -0.041 in 2018. The spatial map of NDVI and NDBI was prepared for three studied years i.e. 1995, 2008, and 2018 (Figure 6). It is possible to discover areas of degradation of land and restoration using NDVI demonstrations for time series analysis (Eckert *et al.*, 2015). A tried-and-true way to determine the NDVI of a certain location is to monitor the prolonged drought and gauge the condition of the greenery (Tariq *et al.*, 2023). NDVI decreased while LST and NDBI both significantly increased in central urban areas (Figure 6).

Table 2. UHI and Non-UHIs statistics.

	In 1995		In 2008		In 2018	
	Mean LST	Area (sq. km)	Mean LST	Area (sq. km)	Mean LST	Area (sq. km)
UHI	33.18	83.78	32.78	88.97	34.48	80.52
Non UHI	28.55	177.22	28.43	172.68	29.54	181.13
UHI intensity	4.63		4.35		4.94	

Table 3. LST and its relationship with LULC.

Land class	LST_1995	LST_2008	LST_2018
Forest	28.425	28.241	29.16
Cultivated land	32.513	32.416	34.5
Urban/built-up	30.129	30.765	31.7
Sand/gravel	30.604	31.302	32.19
Water	25.468	29.170	29.4

Table 4. NDVI and NDBI statistic of years 1995, 2008, and 2018.

S. No.	Date	Minimum		Mean		Maximum		Standard deviation	
		NDVI	NDBI	NDVI	NDBI	NDVI	NDBI	NDVI	NDBI
1	1995 April	-0.232	-0.387	0.116	0.247	0.471	0.613	0.081	0.102
2	2008 April	-0.212	-0.309	0.194	0.377	0.495	0.549	0.092	0.067
3	2018 April	-0.074	-0.289	0.242	-0.041	0.472	0.266	0.072	0.089

Conclusion

In the Hetauda sub-metropolitan city of Nepal, the study found a high rate of urban expansion i.e. 14.9 km^2 of urban/built-up area was more in 2018 compared to 1990. There was the formation of UHI in the industrial area, downtown of Hetauda sub-metropolitan city as well as bare cultivated land and its effect was about 4°C. The LST was higher for urban/built-up and cultivated land use types. Forest and agricultural land was in decreasing trend and converted into urban/built-up areas which again supports the expansion of the UHI. Altogether, the negative correlation between LST and NDVI reveals that green vegetation lowers the LST in an urban area while the positive correlation between LST and NDBI implies that build-up area strengthens LST. Overall, the application of remote sensing and GIS is an effective cost-effective tool for analyzing UHI which will be beneficial for urban planners for sustainable urban planning.

DECLARATIONS

Author contribution statement

Conceptualization: BS and MM; Methodology: BS and AT.; Software and validation: BS; Formal analysis and investigation: BS and AT; Data curation: BS and AT; Writing—original draft preparation: BS, MM, GP; Writing—review and editing: GP, HCJ, and MM; Visualization: BS and MM; Supervision: MM and AT. All authors have read and agreed to the published version of the manuscript

Conflicts of interest: The authors declare that there are no conflicts of interest regarding the publication of this manuscript.

Ethics approval: This study did not involve any animal or human participant and thus ethical approval was not applicable.

Consent for publication: All co-authors gave their consent to publish this paper in AAES.

Data availability: The data that support the findings of this study are available on request from the corresponding author.

Supplementary data: Not available.

Funding statement: Not available.

Additional information: No additional information is available for this paper.

Publisher's Note: Agro Environ Media (AESA) remains neutral with regard to jurisdictional claims in published maps, figures and institutional affiliations.

REFERENCES

Agam, N., Kustas, W. P., Anderson, M. C., Li, F., & Neale, C. M. U. (2007). A vegetation index based technique for spatial sharpening of thermal imagery. *Remote Sensing of Environment*, *107*(4), 545–558.

Agrawal, Y. C., Whitmire, A., Mikkelsen, O. A., & Pottsmith, H. C. (2008). Light scattering by random shaped particles and consequences on measuring suspended sediments by laser diffraction. *Journal of Geophysical Research: Oceans*, *113*(C4).

Barsi, J. A., Lee, K., Kvaran, G., Markham, B. L., & Pedelty, J. A. (2014). The spectral response of the Landsat-8 operational land imager. *Remote Sensing*, *6*(10), 10232–10251.

Bhatti, S. S., & Tripathi, N. K. (2014). Built-up area extraction using Landsat 8 OLI imagery. *GIScience & Remote Sensing*, *51*(4), 445–467.

Bhuyan, M. D. I., Science, M. B., Islam, J., Science, M. B., & Wahid, C. (2013). *Characteristics of Summer Monsoon Rainfall over South Asia Using TRMM Data*. *July*.

CBS. (2011). *Nepal - Population and Housing Census 2011*. https://catalog.ihsn.org/catalog/4210

CBS. (2021). *National Census 2021*. https://web.archive.org/web/20220127132634/https://censusnepal.cbs.gov.np/

Clinton, N., & Gong, P. (2013). MODIS detected surface urban heat islands and sinks: Global locations and controls. *Remote Sensing of Environment*, *134*, 294–304.

Congalton, R. G. (2001). Accuracy assessment and validation of remotely sensed and other spatial information. *International Journal of Wildland Fire*, *10*(4), 321–328.

DFRS. (2015). *State of Nepal ' S Forests* (Issue December). https://doi.org/978-9937-8896-3-6

Eckert, S., Hüsler, F., Liniger, H., & Hodel, E. (2015). Trend analysis of MODIS NDVI time series for detecting land degradation and regeneration in Mongolia. *Journal of Arid Environments*, *113*, 16–28.

Fernández, A., Illera, P., & Casanova, J. L. (1997). Automatic mapping of surfaces affected by forest fires in Spain using AVHRR NDVI composite image data. *Remote Sensing of Environment*, *60*(2), 153–162.

Gao, B. C. (1995). Normalized difference water index for remote sensing of vegetation liquid water from space. *Imaging Spectrometry*, *2480*, 225–236.

Ghosh, J., & Porchelvan, P. (2018). Relationship between surface temperature and land cover types using thermal infrared band and NDVI for Vellore District, Tamilnadu, India. *Nature Environment and Pollution Technology*, *17*(2), 611–617.

Gillespie, T. W., Ostermann-Kelm, S., Dong, C., Willis, K. S., Okin, G. S., & MacDonald, G. M. (2018). Monitoring changes of NDVI in protected areas of southern California. *Ecological Indicators*, *88*, 485–494.

Grigora?, G., & Uri?escu, B. (2019). Land use/land cover changes dynamics and their effects on surface urban heat island in Bucharest, Romania. *International Journal of Applied Earth Observation and Geoinformation*, *80*, 115–126.

Haylemariyam, M. B. (2018). Detection of land surface temperature in relation to land use land cover change: Dire Dawa City, Ethiopia. *J Remote Sens Gis*, *7*(3), 245.

Heinl, M., Hammerle, A., Tappeiner, U., & Leitinger, G. (2015). Determinants of urban–rural land surface temperature differences – A landscape scale perspective. *Landscape and Urban Planning*, *134*, 33–42. https://doi.org/10.1016/J.LANDURBPLAN.2014.10.003

Hokao, K., Phonekeo, V., & Srivanit, M. (2012). Assessing the impact of urbanization on urban thermal environment: A case study of Bangkok Metropolitan. *International Journal of Applied*, *2*(7).

Jamei, Y., Rajagopalan, P., & Sun, Q. C. (2019). Spatial structure of surface urban heat island and its relationship with vegetation and built-up areas in Melbourne, Australia. *Science of the Total Environment*, *659*, 1335–1351.

Jiang, J., & Tian, G. (2010). Analysis of the impact of land use/land cover change on land surface temperature with remote sensing. *Procedia Environmental Sciences*, *2*, 571-575.

Kaplan, G., Avdan, U., & Avdan, Z. Y. (2018). Urban heat island analysis using the landsat 8 satellite data: A case study in Skopje, Macedonia. *Multidisciplinary Digital Publishing Institute Proceedings*, *2*(7), 358.

Laosuwan, T., & Sangpradit, S. (2012). Urban heat island monitoring and analysis by using integration of satellite data and knowledge based method. *International Journal of Development and Sustainability*, *1*(2), 99–110.

Li, B., Wang, W., Bai, L., Wang, W., & Chen, N. (2018). Effects of spatio-temporal landscape patterns on land surface temperature: a case study of Xi'an city, China. *Environmental Monitoring and Assessment*, *190*, 1–11.

Li, W., Saphores, J.-D. M., & Gillespie, T. W. (2015). A comparison of the economic benefits of urban green spaces estimated with NDVI and with high-resolution land cover data. *Landscape and Urban Planning*, *133*, 105–117.

Ma, Y., Kuang, Y., & Huang, N. (2010). Coupling urbanization analyses for studying urban thermal environment and its interplay with biophysical parameters based on TM/ETM+ imagery. *International Journal of Applied Earth Observation and Geoinformation*, *12*(2), 110–118.

Muzzini, E., & Aparicio, G. (2013). *Urban growth and spatial transition in Nepal: An initial assessment*. World Bank Publications.

Nuruzzaman, M. (2015). Urban heat island: causes, effects and mitigation measures-a review. *International Journal of Environmental Monitoring and Analysis*, *3*(2), 67–73.

Rajeshwari, A., & Mani, N. D. (2014). Estimation of land surface temperature of Dindigul district using Landsat 8 data. *International Journal of Research in Engineering and Technology*, *3*(5), 122–126.

Ranagalage, M., Estoque, R. C., Handayani, H. H., Zhang, X., Morimoto, T., Tadono, T., & Murayama, Y. (2018). Relation between urban volume and land surface temperature: A comparative study of planned and traditional cities in Japan. *Sustainability*, *10*(7), 2366.

Ranagalage, M., Estoque, R. C., & Murayama, Y. (2017). An urban heat island study of the Colombo metropolitan area, Sri Lanka, based on Landsat data (1997–2017). *ISPRS International Journal of Geo-Information*, *6*(7), 189.

Rimal, B., Zhang, L., Keshtkar, H., Haack, B. N., Rijal, S., & Zhang, P. (2018). Land use/land cover dynamics and modeling of urban land expansion by the integration of cellular automata and markov chain. *ISPRS International Journal of Geo-Information*, *7*(4), 154.

Rouse, J. W., Haas, R. H., Schell, J. A., & Deering, D. W. (1974). Monitoring vegetation systems in the Great Plains with ERTS. *NASA Spec. Publ*, *351*(1), 309.

Rousta, I., Sarif, M. O., Gupta, R. D., Olafsson, H., Ranagalage, M., Murayama, Y., Zhang, H., & Mushore, T. D. (2018). Spatiotemporal analysis of land use/land cover and its effects on surface urban heat island using Landsat data: A case study of Metropolitan City Tehran (1988–2018). *Sustainability*, *10*(12), 4433.

Sahana, M., Ahmed, R., & Sajjad, H. (2016) Analyzing land surface temperature distribution in response to land use/land cover change using split window algorithm and spectral radiance model in Sundarban Biosphere Reserve, India. *Modeling Earth Systems and Environment*, 2: 81.

Santos, M., & Gerry, C. (2017). *The shared space: The two circuits of the urban economy in underdeveloped countries*. Routledge.

Sarif, M. O., Rimal, B., & Stork, N. E. (2020). Assessment of changes in land use/land cover and land surface temperatures and their impact on surface urban heat island phenomena in the Kathmandu Valley (1988–2018). *ISPRS International Journal of Geo-Information*, *9*(12), 726.

Sharma, R., Chakraborty, A., & Joshi, P. K. (2015). Geospatial quantification and analysis of environmental changes in urbanizing city of Kolkata (India). *Environmental Monitoring and Assessment*, *187*, 1–12.

Shukla, P. R., Skeg, J., Buendia, E. C., Masson-Delmotte, V., Pörtner, H.-O., Roberts, D. C., Zhai, P., Slade, R., Connors, S., & Van Diemen, S. (2019). *Climate Change and Land: an IPCC special report on climate change, desertification, land degradation, sustainable land management, food security, and greenhouse gas fluxes in terrestrial ecosystems*.

Singh, P., Kikon, N., & Verma, P. (2017). Impact of land use change and urbanization on urban heat island in Lucknow city, Central India. A remote sensing based estimate. *Sustainable Cities and Society*, *32*, 100–114.

Stewart, I. D., & Oke, T. R. (2012). Local climate zones for urban temperature studies. *Bulletin of the American Meteorological Society*, *93*(12), 1879–1900.

Tafesse, B., & Suryabhagavan, K. V. (2019). Systematic modeling of impacts of land -use and land-cover changes on land surface temperature in Adama Zuria District, Ethiopia. *Modeling Earth Systems and Environment*, *5*, 805–817.

Tali, J.A., Divya, S., Murthy, K. (2013) Influence of urbanisation on the land use change: A case study of Srinagar City. *American Journal of Research Communication*, 1: 271-283.

Tariq, A., Mumtaz, F., Majeed, M., & Zeng, X. (2023). Spatio-temporal assessment of land use land cover based on trajectories and cellular automata Markov modelling and its impact on land surface temperature of Lahore district Pakistan. *Environmental Monitoring and Assessment*, *195*(1), 114.

Tariq, A., Riaz, I., Ahmad, Z., Yang, B., Amin, M., Kausar, R., Andleeb, S., Farooqi, M. A., & Rafiq, M. (2020). Land surface temperature relation with normalized satellite indices for the estimation of spatio-temporal trends in temperature among various land use land cover classes of an arid Potohar region using Landsat data. *Environmental Earth Sciences*, *79*, 1–15.

Tempfli, K., Huurneman, Gc., Bakker, Wh., Janssen, L. L. F., Feringa, W. F., Gieske, A. S. M., Grabmaier, K. A., Hecker, C. A., Horn, J. A., & Kerle, N. (2009). *Principles of remote sensing: an introductory textbook*. International Institute for Geo-Information Science and Earth Observation.

Thapa, R. B., & Murayama, Y. (2009). Examining spatiotemporal urbanization patterns in Kathmandu Valley, Nepal: Remote sensing and spatial metrics approaches. *Remote Sensing*, *1*(3), 534–556.

Townshend, J. (2001). Landsat Imagery in Geography. *International Encyclopedia of the Social & Behavioral Sciences*, 8265–8270. https://doi.org/10.1016/B0-08-043076-7/02527-4

United Nations. (2018). *World Urbanization Prospects - Population Division - United Nations*. https://population.un.org/wup/

United Nations, (2007). World urbanization prospects.

West, H., Quinn, N., Horswell, M., & White, P. (2018). *Performance of Sentinel-2 NDVI for assessing the relationship between vegetation and soil moisture under extreme drought conditions*. https://uwe-repository.worktribe.com/output/869693/performance-of-sentinel-2-ndvi-for-assessing-the-relationship-between-vegetation-and-soil-moisture-under-extreme-drought-conditions

Wu, C. (2004). Normalized spectral mixture analysis for monitoring urban composition using ETM+ imagery. *Remote Sensing of Environment*, *93*(4), 480–492.

Xiong, L., Deng, Q., Tucker, G. J., McDowell, D. L., & Chen, Y. (2012). Coarse-grained atomistic simulations of dislocations in Al, Ni and Cu crystals. *International Journal of Plasticity*, *38*, 86–101.

Xu, W., Gu, S., Zhao, X., Xiao, J., Tang, Y., Fang, J., Zhang, J., & Jiang, S. (2011). High positive correlation between soil temperature and NDVI from 1982 to 2006 in alpine meadow of the Three-River Source Region on the Qinghai-Tibetan Plateau. *International Journal of Applied Earth Observation and Geoinformation*, *13*(4), 528–535.

Zha, Y., Gao, J., & Ni, S. (2003). Use of normalized difference built-up index in automatically mapping urban areas from TM imagery. *International Journal of Remote Sensing*, *24*(3), 583–594. https://doi.org/10.1080/01431160304987